

The Doping effect of Chalcogen on the Two-Dimensional Ferromagnetic Material Chromium Tribromide

Yanfeng Ge,¹ Qiaoqiao Li,¹ Wenhui Wan,¹ Jian-Min Zhang,² Wenhui Xie,³ and Yong Liu^{1,*}

¹Technology and Key Laboratory for Microstructural Material Physics of Hebei Province, School of Science, Yanshan University, Qinhuangdao, 066004, People's Republic of China

²Fujian Provincial Key Laboratory of Quantum Manipulation and New Energy Materials,

College of Physics and Energy, Fujian Normal University, Fuzhou, 350117, People's Republic of China

³Department of Physics, East China Normal University, Shanghai 200062, People's Republic of China

(Dated: October 23, 2021)

Recently the discovery of magnetic order in two-dimensional monolayer chromium trihalides opens the new research field in two-dimensional materials. We use first-principles calculations to systematically examine the doping effect of chalcogen on CrBr₃. In the case of S-doping, four stable configurations, Cr₂Br₅S, Cr₂Br₄S₂-A, Cr₂Br₄S₂-B and Cr₂Br₃S₃-A, are predicted to be ferromagnetic semiconductors. It is found that the new bands appearing in the original bandgap are made up of S-p and Cr-d-e_g orbitals, lead to the obvious reduce of bandgap and the enhanced optical absorption in the visible range. Due to the decrease of valence electron after chalcogen doping, the magnetic moment also decreases with the increase of S atoms, and the character of ferromagnetic semiconductor is always hold in a wide range of strain. The results shown that monolayer CrBr₃ with chalcogen doping supply a effectual way to control the magnetism and extend the optoelectronic applications.

I. INTRODUCTION

In the last decade, two-dimensional (2D) materials [1–6] have attracted a great deal of attention also been one of the most exciting research fields due to the wealth of physics and promising applications. Besides the earliest graphene, various 2D materials also include hexagonal boron nitride, silicene, transition metal dichalcogenides, MXene and so on. However, the absent of intrinsic magnetism in the most of the available 2D materials with pristine form limits their applications in spintronics and spin-based electronics, particularly information technology. As a consequence, 2D ferromagnetic materials with the combination of large spin polarization and high Curie temperature (T_C) are of particular importance and interest. The simple and direct means to achieve magnetic in 2D materials is dopants of magnetic atoms. However, doping not only destroys the perfect crystalline order, but also the low solubility and surface clustering [7, 8] are the serious problems. Although there are some other strategies to magnetize [9], the long-range magnetic order is rarely observed experimentally in 2D materials. For the theoretical reason, Mermin and Wagner theorem demonstrate the strong fluctuations lead to the absence of long range magnetic order in spin-rotational invariant systems with short range exchange interactions.

Fortunately, the magnetocrystalline anisotropy make some materials be not limited by the Mermin-Wagner theorem. The recent reports of magnetic order in different 2D crystals (Cr₂Ge₂Te₆, CrI₃ and FePS₃) [10–14] mark a milestone in the research of 2D magnetic materials and explore the 2D magnetic physics, indispensable for the low-dimensional spintronics. The small cleavage energy in the ferromagnetic van der Waals (vdW) bulk CrI₃ is propitious to the mechanically exfoliated monolayer structure, prevalent in other common 2D materials. The magnetization experiments show the bulk crys-

tal has the out-of-plane ferromagnetic (FM) order below $T_C = 68$ K [15–17] with weak interlayer coupling. FM order is still residing in the monolayer structure with the lower T_C of 45 K [11]. But the suppressed magnetization occurs in the bilayer CrI₃ due to the metamagnetic effect [18]. The numerous publications with regard to CrI₃ emerge in order to study and manipulate the magnetic properties [19–23]. The temperature-dependent magnetic anisotropy [24] of 2D CrI₃ is contributed from the ferromagnetic super-exchange across the anisotropic Cr-I-Cr bonds and the weak single ion anisotropy of Cr atom [25]. Furthermore, the electric field [26], electrostatic doping [27] and strain [28] are found to control the 2D magnetism of CrI₃. Besides, the homogeneous materials CrBr₃ and CrCl₃ also induce the research interests [29–35] and the bulk CrBr₃ in particular has been studied as ferromagnetic semiconductor with $T_c = 31$ K long ago [29]. And the in-plane multiferroicity [23], such as ferromagnetic and ferroelectricity order, are also discovered in the charged monolayer CrBr₃. The mixed halide series CrCl_{3-x}Br_x realizes the regulation of exchange anisotropy [33] and can be applied to the ultrathin magneto-optical devices [36–38].

In the present work, we focus on the 2D semiconductor CrBr₃ and study the doping effect of chalcogen (S, Se and Te), in consideration of ferromagnetic metal in chromium chalcogens [39, 40] with the same crystal structure as CrI₃. Except the prototype structure of CrBr₃, Six types of doping structure have been constructed with doping concentration of 1 ~ 3 chalcogenide atoms per primitive cell. In the case of Cr₂Br_{6-x}S_x, four of the structures have dynamic stability, verified by the phonon spectra. They are as follows: Cr₂Br₅S, Cr₂Br₄S₂-A, Cr₂Br₄S₂-B and Cr₂Br₃S₃-A. By calculating spin-polarized electronic structures, the four stable configurations are also confirmed as ferromagnetic semiconductor, coordination with CrBr₃. However, there new bands appears in the bandgap of Cr-d-t_{2g} orbit and the number of new bands increases linearly with S atomic content, which impact the global bandgap significantly. Due to the reduce of valence electron, magnetic moment also decreases under

* yongliu@ysu.edu.cn

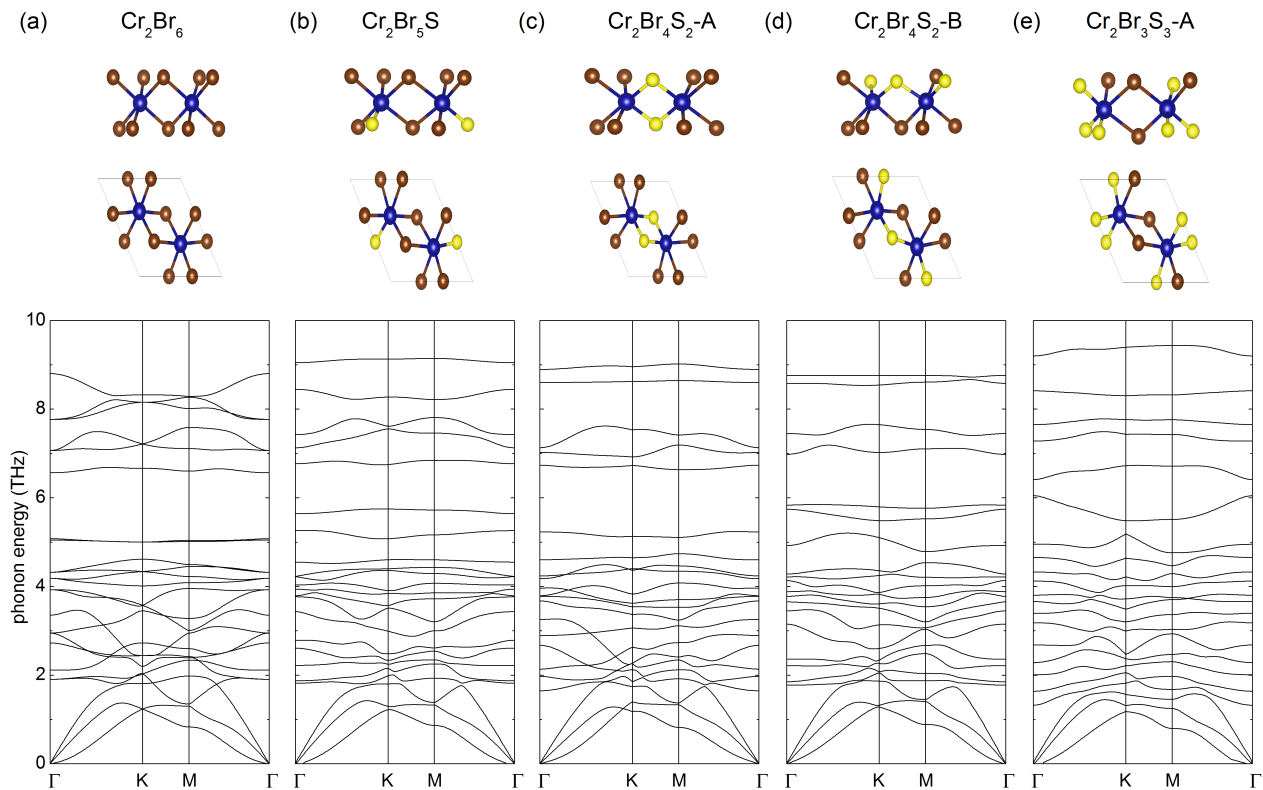


FIG. 1. **Crystal structures and phonon spectra of $\text{Cr}_2\text{Br}_{6-x}\text{S}_x$.** (a) Crystal structure (upper panel) and phonon spectrum (bottom panel) of pristine CrBr_3 , whose primitive cell has two Cr atoms and six Br atoms (Cr_2Br_6). In each primitive cell, Br atoms substituted by (b) one S atom: $\text{Cr}_2\text{Br}_5\text{S}$, (c) two S atoms: $\text{Cr}_2\text{Br}_4\text{S}_2\text{-A}$, (d) two S atoms : $\text{Cr}_2\text{Br}_4\text{S}_2\text{-B}$ and (e) three S atoms: $\text{Cr}_2\text{Br}_3\text{S}_3\text{-A}$.

the doping condition, such as $3 \mu_B$ per $\text{Cr}_2\text{Br}_3\text{S}_3\text{-A}$ primitive cell. These results suggest that monolayer CrBr_3 with chalcogen doping is also robust intrinsic ferromagnetic semiconductor. Moreover, the new energy band can also absorb the low-energy photons and lead to the optical absorption in the visible range increases, which makes CrBr_3 with chalcogen doping to be possible candidates for optoelectronic applications.

II. METHODS

Technical details of the calculations are as follows. All calculations of electronic structures and optical properties accurately were carried out using the Vienna ab initio simulation package (VASP) code [41, 42] within the projector augmented-wave (PAW) method [43, 44] and the exchange correlation functional of General gradient approximation (GGA) in the Perdew-Burke-Ernzerhof (PBE) implementation [45]. The thickness of the vacuum gap is at least 15 \AA , which is large enough to avoid the interlayer interactions in the periodic structure. By requiring convergence of results, the kinetic energy cutoff of 500 eV and the Monkhorst-Pack k -mesh of $16 \times 16 \times 1$ were used in all calculations about the electronic ground-state properties. The phonon spectra was calculated on a $4 \times 4 \times 1$ q -grid using the density functional perturbation theory (DFPT) [46] with VASP and Phonopy

codes [47]. The biaxial strain was introduced by adjusting the lattice constant a with the strain capacity $\varepsilon = (a - a_0)/a_0 \times 100 \%$, where a_0 is equilibrium lattice constant. The equilibrium lattice constant of the monolayer CrBr_3 was found to be $a_0 = 6.43 \text{ \AA}$.

III. RESULTS

Now we discuss the possible lattice structures of $\text{Cr}_2\text{Br}_{6-x}\text{S}_x$ with $x = 1 \sim 3$. First, the hexagonal honeycomb primitive cell of CrBr_3 has eight atoms with each Cr surrounded by six Br atoms [Fig. 1(a)]. Due to the equivalency of six Br atoms in the primitive cell, $\text{Cr}_2\text{Br}_5\text{S}$ has only one structure, as shown in Fig. 1(b). For the case of two S atoms, there are three different structures, marked by $\text{Cr}_2\text{Br}_4\text{S}_2\text{-A}$ [Fig. 1(c)], $\text{Cr}_2\text{Br}_4\text{S}_2\text{-B}$ [Fig. 1(d)] and $\text{Cr}_2\text{Br}_4\text{S}_2\text{-C}$ (see Appendix A) for simplicity, corresponding to the adjacency, alternation and para-position in the top-view of $\text{Cr}_2\text{Br}_{6-x}\text{S}_x$, respectively. And there are two structures for the case of three S atoms. One is shown in Fig. 1(e) with three S atoms locating at the top and bottom edges of Cr atoms, $\text{Cr}_2\text{Br}_3\text{S}_3\text{-A}$. The other one have three ipsilateral S atoms, $\text{Cr}_2\text{Br}_3\text{S}_3\text{-B}$ (see Appendix A), similar to the Janus monolayer structure of transition metal dichalcogenide [48]. The doping of S atom lead to the slight decrease of equilibrium lattice constant, as shown

in Tab. I. Furthermore, the calculations of phonon spectra are applied to ensure the stability. The absent of imaginary frequency in the phonon spectrum of Cr_2Br_6 illustrates the dynamic stability of prototype structure, consistent with the previous works [32]. After the doping of S atom, it is found that not all cases have stability. $\text{Cr}_2\text{Br}_5\text{S}$, $\text{Cr}_2\text{Br}_4\text{S}_2\text{-A}$, $\text{Cr}_2\text{Br}_4\text{S}_2\text{-B}$ and $\text{Cr}_2\text{Br}_3\text{S}_3\text{-A}$ are stable as shown in Fig. 1, contrary to the other cases (see Appendix A).

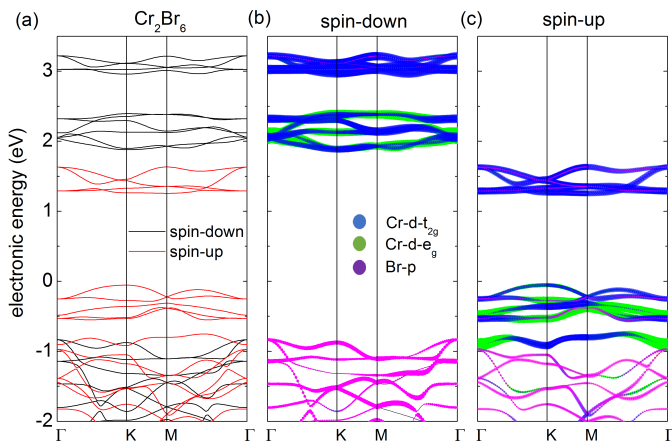


FIG. 2. **Band structures of Cr_2Br_6 .** (a) Spin-polarized band structure of Cr_2Br_6 . The red (black) lines represent the band structure in the spin-up (spin-down) direction. (b) Projected band structures in the spin-down direction and (c) spin-up direction of Cr- t_{2g} (blue circle), Cr- e_g orbits (green circle) and Br-p orbit (purple circle).

The results of electronic structure show that monolayer Cr_2Br_6 is ferromagnetic semiconductor with the bandgap of 1.32 eV [Fig. 2(a)], in coordination with the previous work [32]. The conduction band minimum (CBM) of band structure in the spin-down direction mainly consist of the $d-t_{2g}$ orbit of Cr atom as well as p orbit of Br atom contributing the valence band maximum (VBM) [Fig. 2(b)]. For the case of spin-up direction [Fig. 2(c)], CBM are also $d-t_{2g}$ orbit, but VBM is composed of $d-t_{2g}$ and $d-e_g$ orbits of Cr atom, clearly different from the spin-down direction. And the band structure of spin-up direction provides the global bandgap, much lower than that in spin-down direction [Tab. I]. Due to the ferromagnetic semiconductor, integral magnetic moment is also obtained with the value of $6 \mu_B$ per primitive cell [Tab. I], which are from $3 \mu_B$ of each Cr atom.

TABLE I. The characteristic parameter of electronic structure.

	a_0 Å	bandgap _{up} (eV)	bandgap _{down} (eV)	magnetic moment (μ_B / primitive cell)
Cr_2Br_6	6.43	1.32	2.72	6.0
$\text{Cr}_2\text{Br}_5\text{S}$	6.37	0.79	2.29	5.0
$\text{Cr}_2\text{Br}_4\text{S}_2\text{-A}$	6.31	0.54	2.05	4.0
$\text{Cr}_2\text{Br}_4\text{S}_2\text{-B}$	6.32	0.44	1.93	4.0
$\text{Cr}_2\text{Br}_3\text{S}_3\text{-A}$	6.28	0.17	1.60	3.0
$\text{Cr}_2\text{Br}_5\text{Se}$	6.36	0.79	2.27	5.0

We then study the doping effect of S atom on the elec-

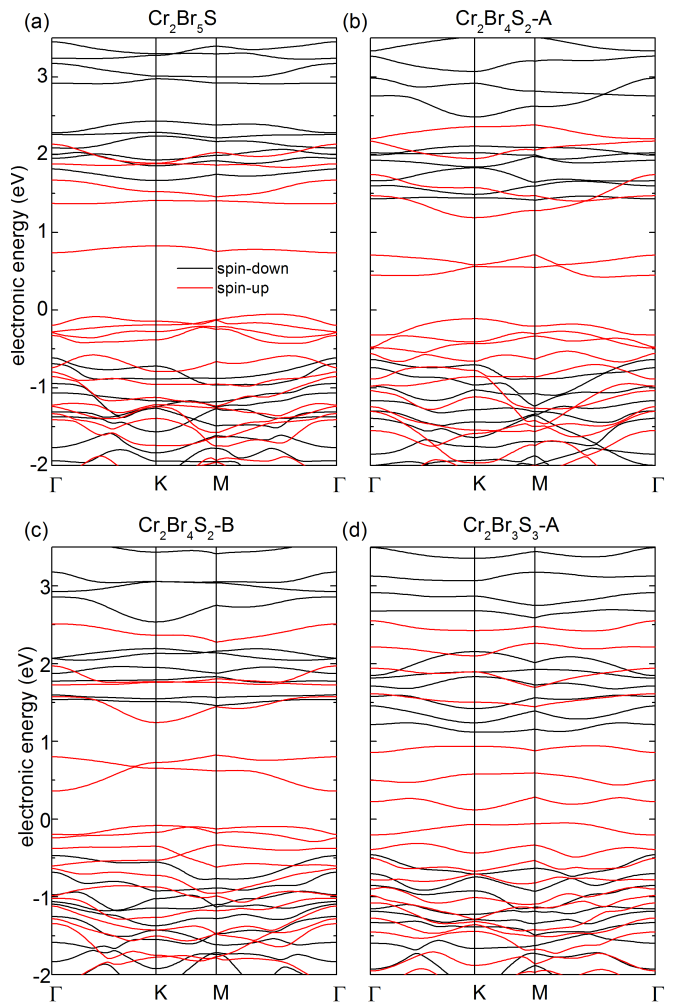


FIG. 3. **Band structures of $\text{Cr}_2\text{Br}_{6-x}\text{S}_x$.** (a) Spin-polarized band structure of $\text{Cr}_2\text{Br}_5\text{S}$, (b) $\text{Cr}_2\text{Br}_4\text{S}_2\text{-A}$, (c) $\text{Cr}_2\text{Br}_4\text{S}_2\text{-B}$ and (d) $\text{Cr}_2\text{Br}_3\text{S}_3\text{-A}$. It's pretty obvious that the band gap decreases with the increase of S atoms.

tronic structure of Cr_2Br_6 . All the four stable structures of $\text{Cr}_2\text{Br}_{6-x}\text{S}_x$ have the ferromagnetic ground state as same as Cr_2Br_6 and the ferromagnetic band structure are shown in Fig. 3. It is obviously found that the global bandgap, spin-up direction, decreases rapidly with the increase in numbers of substitutional S atoms and reduces to a fairly low value of 0.17 eV in $\text{Cr}_2\text{Br}_3\text{S}_3\text{-A}$. The reduce of bandgap also occurs in the case of spin-down direction, as summarized in Tab. I. The projected band structures of $\text{Cr}_2\text{Br}_5\text{S}$ show that S atom primarily influences the band structure in the spin-up direction [Fig. 4]. A new energy band presents in the energy gap between of Cr- $d-t_{2g}$ orbits and is contributed by the p orbit of S atom and $d-e_g$ orbit of Cr atom. The new bands in the energy range of $0 \sim 1$ eV for other cases are all the results from the same reason. And the effect of S atoms is also reflected by the magnetic moment, which decreases linearly with increase of S atoms. For example, there are still $3 \mu_B$ per $\text{Cr}_2\text{Br}_3\text{S}_3\text{-A}$ primitive cell [Tab. I]. The main reason is that the decrease of valence elec-

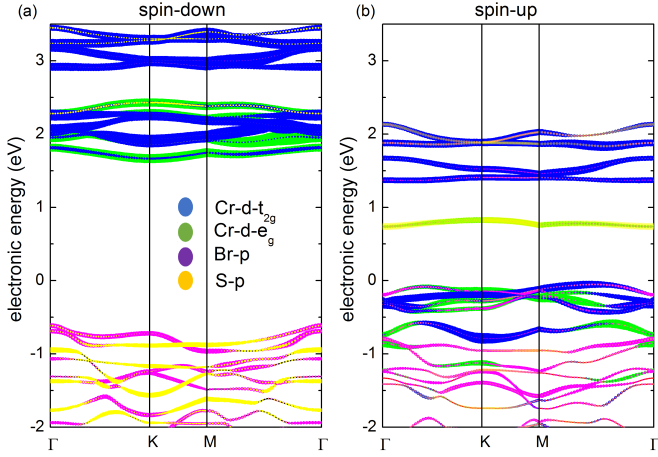


FIG. 4. **Band structures of $\text{Cr}_2\text{Br}_5\text{S}$.** (a) Projected band structures in the spin-down direction and (c) spin-up direction of Cr- t_{2g} (blue circle), Cr- e_g orbits (green circle), Br-p orbit (purple circle) and S-p orbit (yellow circle).

trons after S substitutions impact the occupation numbers on the magnetic Cr-d orbit. The results suggest that monolayer $\text{Cr}_2\text{Br}_{6-x}\text{S}_x$ are also robust intrinsic ferromagnetic semiconductor with different magnetic moments.

Because the possible lattice mismatching with the substrates in the different experimental preparations lead to the present of strain inevitably, the strain is also considered to study the stability of ferromagnetic semiconductor and the modulation of strain. The variation of bandgap under biaxial strains is displayed in Fig. 5(a). The bandgap of $\text{Cr}_2\text{Br}_{6-x}\text{S}_x$ is robust to the biaxial strain obviously, and the bandgap of $\text{Cr}_2\text{Br}_5\text{S}$ has the minimum change. The result of magnetic moment also illustrates that $\text{Cr}_2\text{Br}_{6-x}\text{S}_x$ maintains the character of ferromagnetic semiconductor in a wide range of strain. Beyond S atom, we also consider the effect of heavier chalcogen (Se and Te) in the same structures as above. But it is found that only $\text{Cr}_2\text{Br}_5\text{Se}$ has structural stability, as shown in Fig. 6, while imaginary frequency exists in other situations, as summarized in Tab. II. The electronic structures show that $\text{Cr}_2\text{Br}_5\text{Se}$ is also ferromagnetic semiconductor and has a bandgap close to $\text{Cr}_2\text{Br}_5\text{S}$. Similarly, the new band in the range of $0 \sim 1$ eV also contributes from the Se-p and Cr-d- e_g orbits.

In addition, we have also calculated the doping effect on the optical properties of Cr_2Br_6 with chalcogen. As shown

TABLE II. Imaginary frequency in unit of THz of the unstable structures.

	S	Se	Te
$\text{Cr}_2\text{Br}_5\text{X}$	stable	stable	-0.09
$\text{Cr}_2\text{Br}_4\text{X}_2\text{-A}$	stable	-0.05	-0.08
$\text{Cr}_2\text{Br}_4\text{X}_2\text{-B}$	stable	-0.04	-0.12
$\text{Cr}_2\text{Br}_4\text{X}_2\text{-C}$	-0.32	-0.03	-0.12
$\text{Cr}_2\text{Br}_3\text{X}_3\text{-A}$	stable	-0.07	-0.09
$\text{Cr}_2\text{Br}_3\text{X}_3\text{-B}$	-0.06	-0.08	-1.60

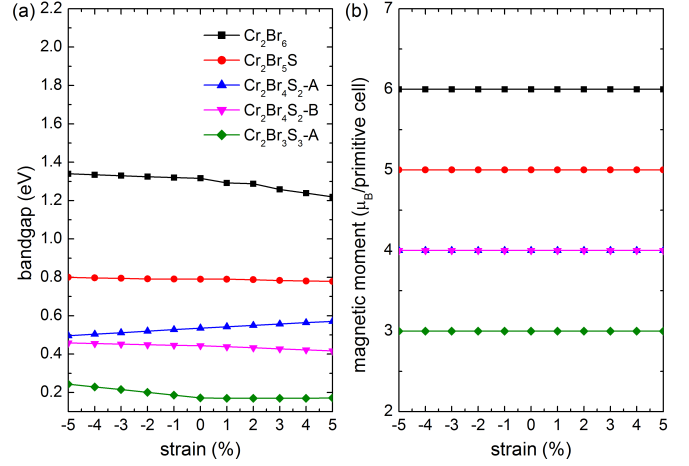


FIG. 5. **Strain effects.** (a) The strain dependence of bandgap and (b) magnetic moment of $\text{Cr}_2\text{Br}_{6-x}\text{S}_x$.

in Fig. 7(a), the in-plane isotropic optical absorption spectra of xy plane distinct from that along the z axis because of the hexagonal symmetry of Cr_2Br_6 . The onset peak around 1.3 eV in Cr_2Br_6 can be traced back to the excitation from valence band to lowest conduction band in the spin-up subband [Fig. 2(c)]. And the most obvious result after the doping is the break of in-plane isotropy, as shown in Fig. 7(b-f), due to the position deviation of S or Se atom relative to Br atom in prototypical Cr_2Br_6 [Fig. 1]. Assisted by the new energy band in the original bandgap of spin-up subband, electronic transition can absorb the low-energy photons, so that the optical absorption of all doping cases in the visible range increases, especially $\text{Cr}_2\text{Br}_4\text{S}_2\text{-A}$ and $\text{Cr}_2\text{Br}_3\text{S}_3\text{-A}$. This illustrates that Cr_2Br_6 with S and Se doping are possible candidates for optoelectronic applications.

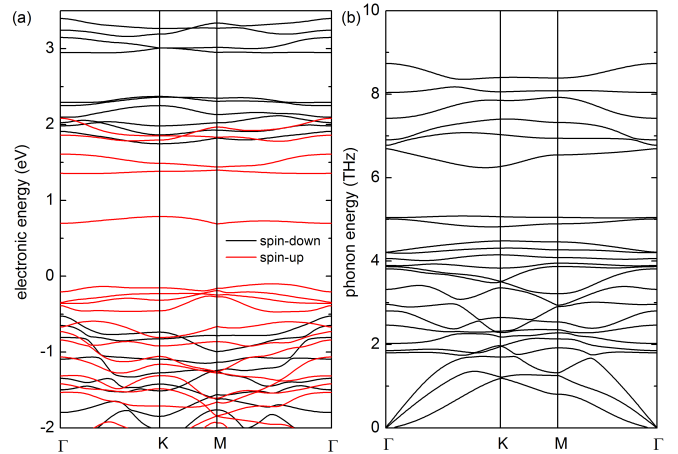


FIG. 6. **Band structure and phonon spectrum of $\text{Cr}_2\text{Br}_5\text{Se}$.**

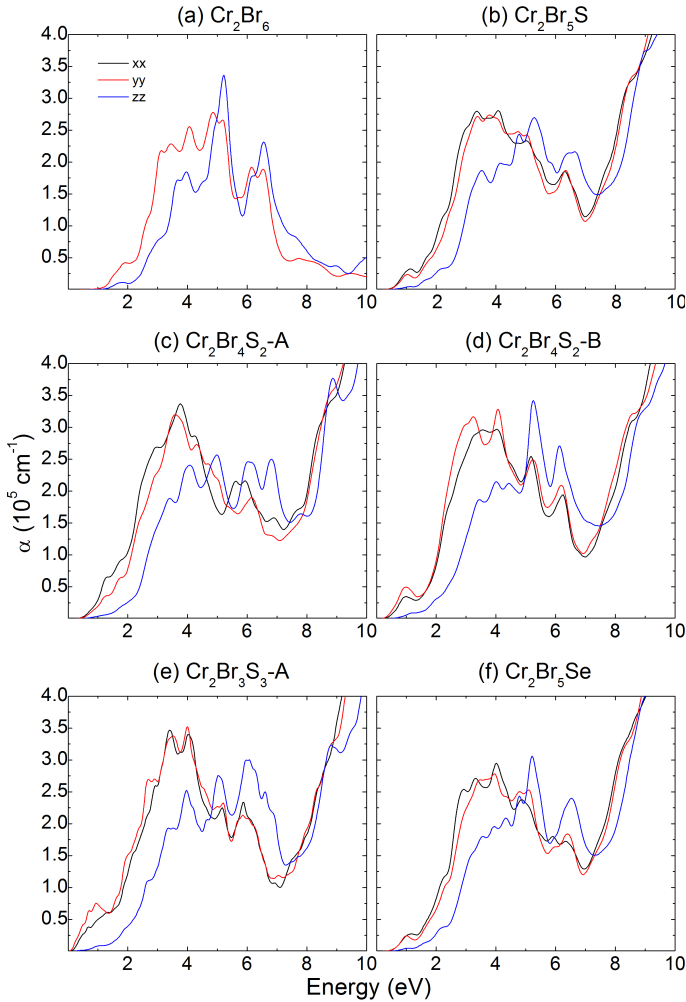


FIG. 7. **Optical absorption spectra.** (a) Cr_2Br_6 , (b) $\text{Cr}_2\text{Br}_5\text{S}_1$, (c) $\text{Cr}_2\text{Br}_4\text{S}_2\text{-A}$, (d) $\text{Cr}_2\text{Br}_4\text{S}_2\text{-B}$, (e) $\text{Cr}_2\text{Br}_3\text{S}_3\text{-A}$ and (f) $\text{Cr}_2\text{Br}_5\text{Se}_1$.

IV. DISCUSSION

We have investigated the doping effect of chalcogen (S, Se and Te) on the CrBr_3 using first-principles calculations. We now take $\text{Cr}_2\text{Br}_{6-x}\text{S}_x$ as the example to summarize our results. Four stable configurations are predicted to be ferromagnetic semiconductors: $\text{Cr}_2\text{Br}_5\text{S}$, $\text{Cr}_2\text{Br}_4\text{S}_2\text{-A}$, $\text{Cr}_2\text{Br}_4\text{S}_2\text{-B}$ and $\text{Cr}_2\text{Br}_3\text{S}_3\text{-A}$. After the doping of S atom, the new bands appearing in the energy range of $0 \sim 1$ eV are made up of S-p and Cr-d- e_g orbitals and lead to the obvious reduce of bandgap in the spin-up direction. Since the change of valence electron, the magnetic moment also decreases with the increase of S atoms, such as $\text{Cr}_2\text{Br}_3\text{S}_3\text{-A}$ has the minimum magnetic moment of $3 \mu_B$ per primitive cell. And the character of ferromagnetic semiconductor is always hold in a wide range of strain. Furthermore, the doping of chalcogen can also lead to the increase of optical absorption in the visible range and make it to be possible candidates for optoelectronic applications.

As an important material in FM semiconductor, CrI_3 is con-

sidered certainly, but we do not find any stable structures, as shown in Appendix B. Except for the substitution, we also calculate the case of atomic adds because of the vacancy at the lattice vertex [Fig. 1]. The large imaginary frequency also explain the structural instability of $\text{Cr}_2\text{Br}_6\text{S}$ and $\text{Cr}_2\text{Br}_6\text{Se}$ (see Appendix C). For the unstable structures, especially the structures with very small imaginary frequency, such as the Janus $\text{Cr}_2\text{Br}_3\text{S}_3\text{-B}$ and $\text{Cr}_2\text{I}_5\text{S}$, maybe prepared in the experiments with the help of substrate, which can enhance 2D material stability. Importantly, we have shown that monolayer CrBr_3 with chalcogen doping is also robust intrinsic ferromagnetic semiconductor and supply an effectual way to control the magnetism and optic properties of monolayer CrBr_3 , which is the current experiments desperately needed.

ACKNOWLEDGMENTS

This work was supported by the NSFC (Grants No.11747054 and No.11874113), the Specialized Research Fund for the Doctoral Program of Higher Education of China (Grant No.2018M631760), the Project of Hebei Educational Department, China (No. ZD2018015 and QN2018012), and the Advanced Postdoctoral Programs of Hebei Province (No.B2017003004).

Appendix A: Unstable structures of $\text{Cr}_2\text{Br}_{6-x}\text{S}_x$

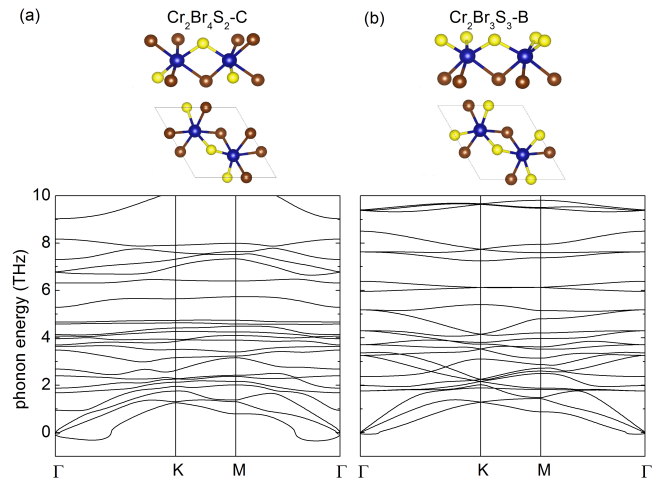


FIG. A1. **Crystal structures and phonon spectra of $\text{Cr}_2\text{Br}_4\text{S}_2\text{-C}$ and $\text{Cr}_2\text{Br}_3\text{S}_3\text{-B}$.**

It is found that two of the crystal structures $\text{Cr}_2\text{Br}_{6-x}\text{S}_x$ considered in the present work are unstable, ensured by the imaginary frequency around Γ point, as shown in Fig. A1. And the value of imaginary frequency in $\text{Cr}_2\text{Br}_3\text{S}_3\text{-B}$ is smaller than that of $\text{Cr}_2\text{Br}_4\text{S}_2\text{-C}$ as well as the distribution of imaginary frequency.

Appendix B: $\text{Cr}_2\text{I}_{6-x}\text{S}_x$

The doping effect of chalcogen is also calculated in the CrI_3 system. But we haven't obtained any stable structure and figure. A2 only plots the phonon spectra of $\text{Cr}_2\text{I}_5\text{S}$ and $\text{Cr}_2\text{I}_4\text{S}_2\text{-A}$ with small imaginary frequency around Γ point.

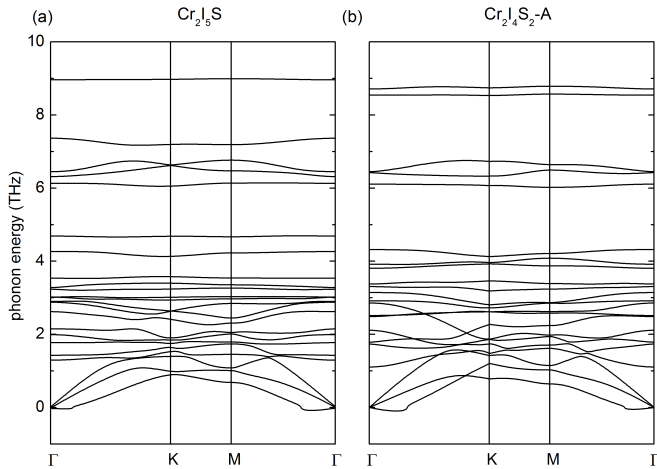


FIG. A2. Phonon spectra of $\text{Cr}_2\text{I}_5\text{S}$ and $\text{Cr}_2\text{I}_4\text{S}_2\text{-A}$.

Appendix C: $\text{Cr}_2\text{Br}_6\text{S}$ and $\text{Cr}_2\text{Br}_6\text{Se}$

The addition of chalcogen is also calculated in the CrBr_3 system. But there are large imaginary frequency in the phonon spectra, as shown in Fig. A3.

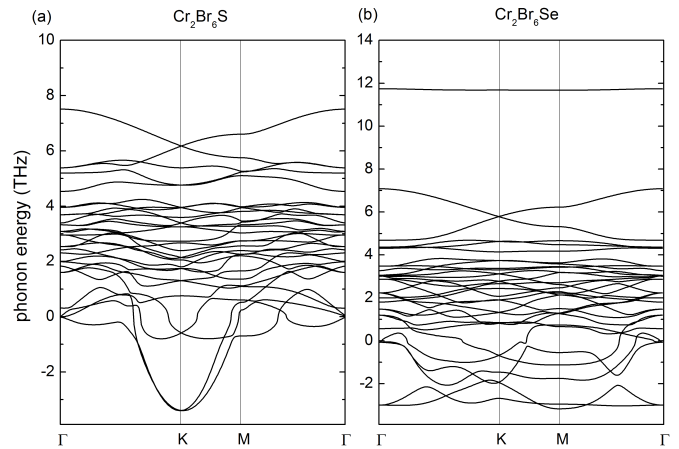


FIG. A3. Phonon spectra of $\text{Cr}_2\text{Br}_6\text{S}$ and $\text{Cr}_2\text{Br}_6\text{Se}$.

- [1] K. S. Novoselov, A. K. Geim, S. V. Morozov, D. Jiang, M. I. Katcnelson, I. V. Grigorieva, S. V. Dubonos, and A. A. Firsov, *Nature* 438, 197 (2005).
- [2] Y. Zhang, Y.-W. Tan, H. L. Stormer, and P. Kim, *Nature* 438, 201 (2005).
- [3] A. K. Geim and I. V. Grigorieva, *Nature* 499, 419 (2013).
- [4] J. Kim, S. S. Baik, S. H. Ryu, Y. Sohn, S. Park, B.-G. Park, J. Denlinger, Y. Yi, H. J. Choi, and K. S. Kim, *Science* 349, 723 (2015).
- [5] X. Xi, Z. Wang, W. Zhao, J.-H. Park, K. T. Law, H. Berger, L. Forro, J. Shan, and K. F. Mak, *Nat. Phys.* 12, 139 (2016).
- [6] Y. Saito, Y. Nakamura, M. S. Bahramy, Y. Kohama, J. Ye, Y. Kasahara, Y. Nakagawa, M. Onga, M. Tokunaga, T. Nojima, Y. Yanase, and Y. Iwasa, *Nat. Phys.* 12, 144 (2016).
- [7] Q. Wang, Q. Sun and P. Jena, *Phys. Rev. Lett.* 95, 167202 (2005).
- [8] T. Dietl, *Nat. Mater.* 9, 965-974 (2010).
- [9] W. Han, R. K. Kawakami, M. Gmitra and J. Fabian, *Nat. Nanotechnol.* 9, 794 (2014).
- [10] C. Gong, L. Li, Z. Li, H. Ji, A. Stern, Y. Xia, T. Cao, W. Bao, C. Wang, Y. Wang, Z. Q. Qiu, R. J. Cava, S. G. Louie, J. Xia, and X. Zhang, *Nature* 546, 265 (2017).
- [11] B. Huang, G. Clark, E. Navarro-Moratalla, D. R. Klein, R. Cheng, K. L. Seyler, D. Zhong, E. Schmidgall, M. A. McGuire, D. H. Cobden, W. Yao, D. Xiao, P. Jarillo-Herrero, and X. Xu, *Nature* 546, 270 (2017).
- [12] X. Wang, K. Du, Y. Y. F. Liu, P. Hu, J. Zhang, Q. Zhang, M. H. S. Owen, X. Lu, C. K. Gan, P. Sengupta, et al., *2D Materials* 3, 031009 (2016).
- [13] J.-U. Lee, S. Lee, J. H. Ryoo, S. Kang, T. Y. Kim, P. Kim, C.-H. Park, J.-G. Park, and H. Cheong, *Nano Letters* 16, 7433 (2016).
- [14] Z. Wang, I. Gutierrez-Lezama, N. Ubrig, M. Kroner, M. Gibertini, T. Taniguchi, K. Watanabe, A. Imamoglu, E. Giannini, A. F. Morpurgo, *Nature Communication* 9, 2516 (2018).
- [15] M. A. McGuire, H. Dixit, V. R. Cooper, and B. C. Sales, *Chem. Mater.* 27, 612 (2015).
- [16] W. N. Hansen, *J. Appl. Phys.* 30, S304 (1959).
- [17] J. F. Dillon, Jr. and C. E. Olson, *J. Appl. Phys.* 36, 1259 (1965).
- [18] E. Stryjewski, N. Giordano, *Metamagnetism. Adv. Phys.* 26, 487 (1977).
- [19] D. R. Klein, D. Macneill, J. L. Lado, et al. *Science* 360, 6394 (2018).
- [20] T. Song, X. Cai, W. Y. Tu, et al. *Science* eaar4851 (2018).
- [21] A. Frisk, L. B. Duffy, S. Zhang, G. van der Laan, T. Hesjedal, *Materials Letters*, 232, 5 (2018).
- [22] P. Jiang, L. Li, Z. Liao, Y. X. Zhao, and Z. Zhong, *Nano Letters* 18, 3844 (2018).
- [23] C. Huang, Y. Du, H. Wu, H. Xiang, K. Deng, and E. Kan, *Phys. Rev. Lett.* 120, 147601 (2018).
- [24] N. Richter, et al. *Physical Review Materials* 2, 2 (2018).
- [25] J. L. Lado, and J. Fernandezrossier, *2d Materials* 4, 3 (2017).
- [26] B. Huang, G. Clark, D. R. Klein, et al. *Nature Nanotechnology*, 13, 544 (2018).
- [27] S. Jiang, L. Li, Z. Wang, et al. *Nature Nanotechnology*, 13, 549 (2018).
- [28] F. Zheng, J. Zhao, Z. Liu, et al. *Nanoscale* 10, 14298 (2018).
- [29] I. Tsubokawa, *J. Phys. Soc. Jpn.* 15, 1664 (1960).
- [30] H. Wang, V. Eyert and U. Schwingenschlogl, *J. Phys.: Condens. Matter* 23 116003 (2011).
- [31] J. Liu, Q. Sun, Y. Kawazoe, P. Jena, *Phys. Chem. Chem. Phys.* 18, 8777 (2016).
- [32] W.-B. Zhang, Q. Qu, P. Zhu, C.-H. Lam, *J. Mater. Chem. C*, 3, 12457 (2015).

- [33] M. Abramchuk, S. Jaszewski, K. R. Metz, G. B. Osterhoudt, Y. Wang, K. S. Burch, and F. Tafti, *Adv. Mater.* 30, 1801325 (2018).
- [34] S.-S. Li, Y.-P. Wang, S.-J. Hu, D. Chen, C.-W. Zhang and S.-S. Yan, *Nanoscale* (2018).
- [35] M. A. McGuire, G. Clark, K. C. Santosh, W. M. Chance, G. E. Jellison, Jr., V. R. Cooper, X. Xu, and B. C. Sales, *Phys. Rev. Materials* 1, 014001 (2017).
- [36] D. Zhong, K. L. Seyler, X. Linpeng, R. Cheng, N. Sivadas, B. Huang, E. Schmidgall, T. Taniguchi, K. Watanabe, M. A. McGuire, W. Yao, D. Xiao, K.-M. C. Fu, X. Xu, *Sci. Adv.* 3, e1603113 (2017).
- [37] Y. Wang, X. Sun, Z. Chen, Y.-Y. Sun, S. Zhang, T.-M. Lu, E. Wertz, J. Shi, *Adv. Mater.* 29, 1702643 (2017).
- [38] K. L. Seyler, D. Zhong, D. R. Klein, S. Gao, X. Zhang, B. Huang, E. Navarro-Moratalla, L. Yang, D. H. Cobden, M. A. McGuire, W. Yao, D. Xiao, P. Jarillo-Herrero, X. Xu, *Nat. Phys.* 14, 277 (2018).
- [39] J. He, and S. Li, *Computational Materials Science* 152, 151 (2018).
- [40] C. Wang, X. Zhou, Y. Pan, J. Qiao, X. Kong, C.-C. Kaun, and W. Ji, *Phys. Rev. B* 97, 245409 (2018).
- [41] G. Kresse and J. Furthmuller, *Comput. Mater. Sci.* 6, 15 (1996).
- [42] G. Kresse and J. Furthmuller, *Phys. Rev. B* 54, 11169 (1996).
- [43] P. E. Blochl, *Phys. Rev. B* 50, 17953 (1994).
- [44] G. Kresse and D. Joubert, *Phys. Rev. B* 59, 1758 (1999).
- [45] J. P. Perdew, K. Burke and M. Ernzerhof, *Phys. Rev. Lett.* 77, 3865 (1996).
- [46] S. Baroni, S. D. Gironcoli, A. D. Corso and P. Giannozzi, *Rev. Mod. Phys.* 73, 515 (2001).
- [47] A. Togo, F. Oba and I. Tanaka, *Phys. Rev. B* 78, 134106 (2008).
- [48] A.-Y. Lu, H. Zhu, J. Xiao, C.-P. Chuu, Y. Han, M.-H. Chiu, C.-C. Cheng, C.-W. Yang, K.-H. Wei, Y. Yang, Y. Wang, D. Sokaras, D. Nordlund, P. Yang, D. A. Muller, M.-Y. Chou, X. Zhang and L.-J. Li, *Nat. Nanotechnol.* 12, 744 (2017).